156 KSME Journal, Vol. 9, No. 2, pp. 156~166, 1995

Two-Dimensional Hyperbolic Heat Conduction in an Orthotropic Medium

Woo-Seung Kim* and Kwan-Soo Lee*

(Received June 7, 1994)

Many natural and man-made materials have the properties of varying thermal conductivity with directions. In the present work, the very short-time temperature response characteristics are examined by using a hyperbolic heat conduction model in an orthotropic medium when an axially symmetric heat flux with a temporal profile, which is either continuous or activated for period Δt, is applied. The ratio of the thermal conductivities is one of the important parameters to be considered. The non-Fourier temperature responses in the orthotropic medium are compared with those in the isotropic case. The Fourier's results are also included and compared with the non-Fowrier's results.

Key Words: Orthotropic Medium, Non-Fourier, Fourier Solution, Thermal Wave

1. Introduction

The hyperbolic heat conduction equation accounts for the thermal inertia of a material since a short time must pass prior to the commencement of heat flow. While the heat conduction equation based on Fourier's law is appropriate for most engineering situations, it fails to adequately predict temperatures in situations which involve very short times, high heat fluxes and cryogenic temperatures. For these situations, the following hyperbolic constitutive law has been proposed,

$$\tau \frac{\partial \vec{q}}{\partial t} + \vec{q} = -k \nabla T \tag{1}$$

which is actually a linearized version of a general theory originally derived by Maxwell(1867). The salient feature of the thermal wave model lies in the involvement of the thermal relaxation time τ which is essentially a measure of the thermal communication time between points in the heated medium. Eq. (1) can be reduced to Fourier's law as the relaxation time τ becomes zero. A typical value of the relaxation time for metals has been reported to be on the order of 10^{-11} second(Gembarovic and Majernik, 1987). Recent work by Kaminski(1990) on nonhomogeneous inner structure materials revealed values of τ on the order of fractions of a minute.

Peshkov(1944) was the earliest investigator to detect experimentally thermal waves of 19 m/sec using the superfluid liquid helium at 1.4 K. Since then, the wave nature of the heat propagation has been the subject of numerous investigations. Baumeister and Hamill(1969) determined the effect of the propagation velocity of heat on the temperature and heat flux distribution in a semi-infinite body due to a step change of surface temperature. Frankel et al.(1987) presented a general one-dimensional temperature and heat flux formulation for hyperbolic heat conduction in a composite medium. Several studies(Glass et al., 1986, Glass et al., 1985, Glass et al., 1990) have been conducted numerically to accommodate the nonlinearities resulting from the temperature-dependent thermal conductivity and the radiation effects. Recently, Tzou(1989, 1990) investigated the thermal shock wave phenomena due to the thermal energy accumulation in a preferential direction using the wave theory for heat conduction.

*Department of Mechanical Engineering, Hanyang University, 17, Haengdang-dong Sungdong-gu, Seoul, 133-791

From the works mentioned above, one can see that significant amount of research effort has been devoted to the thermal wave propagation for an isotropic medium. However, the results of such analyses are not applicable to a non-isotropic medium such as crystals, metals that have undergone heavy cold pressing, heat shielding materials for space vehicles, fiber reinforced structures, and many others(Ozisik, 1993).

As a continuation of the previous work(Kim et al., 1990), the present study is concerned with the temperature response in an orthotropic, semi-infinite medium due to axisymmetric surface sources which are either continuous or single pulses activated for a small period Δt. The spatial profile of the pulses may be either Gaussian, doughnut, or a mixture of Gaussian and doughnut modes. The material properties are assumed to be constant, and radiative and convective losses from the surface are also assumed to be negligible.

2. Problem Formulation

We consider an axisymmetric orthotropic medium in which two dimensional heat conduction and constant thermal properties prevail.

The two-dimensional heat conduction equation with cylindrical symmetry is written as

$$-\frac{1}{r}\frac{\partial}{\partial r}(rq_r)-\frac{\partial q_z}{\partial z}=\rho c_p\frac{\partial T}{\partial t} \tag{2}$$

where r is the radial coordinate, z is the axial coordinate, q_r and q_z are the radial and axial heat flux components, respectively, ρ is the density, and c_p is the specific heat. The modified non-Fourier heat flux laws in an axisymmetric orthotropic medium for the radial and axial heat flux components q_r and q_z are, respectively,

$$\tau\frac{\partial q_r}{\partial t}+q_r=-k_r\frac{\partial T}{\partial r} \tag{3}$$

$$\tau\frac{\partial q_z}{\partial t}+q_z=-k_z\frac{\partial T}{\partial z} \tag{4}$$

where τ is the thermal relaxation time, and k_r and k_z are the radial and axial thermal conductivities, respectively. Eliminating the heat flux components between Eq. (2), and (3) and (4) gives the following hyperbolic heat conduction equation governing the temperature distribution in an orthotropic medium,

$$\frac{1}{r}\frac{\partial}{\partial r}\left(r\frac{\partial T}{\partial r}\right)+\frac{k_z}{k_r}\frac{\partial^2 T}{\partial z^2}=\frac{\tau}{\alpha_r}\frac{\partial^2 T}{\partial t^2}+\frac{1}{\alpha_r}\frac{\partial T}{\partial t} \tag{5}$$

We assume that the region is initially in equilibrium at temperature To and the surface of the medium is irradiated by a source with specified spatial and temporal profiles. The heat flux to the surface of the medium is taken as

$$q_z=q_o f(t)\left[A+(1-A)\frac{r^2}{d^2}\right]e^{-\frac{r^2}{d^2}} \quad at\ z=0 \tag{6}$$

where q_0 is a scaling factor which corresponds to the maximum incident flux for the Gaussian source. The parameter d is a characteristic radial dimension and $f(t)$ represents the temporal profile of the heat flux which is dimensionless. The parameter A represents the fraction of the flux that contains the Gaussian mode and is written as

$$A=\frac{TEM_{00}}{TEM_{00}+TEM_{01}} \tag{7}$$

where A falls in the range $0\le A\le 1$. For situations which involve laser beam irradiation of a surface, it is appropriate to consider the spatial profile of the impinging beam in a heat conduction analysis. For example, most pulsed solid state lasers operate in the lowest-order spatial mode which is known as TEM_{00}(Transverse electromagnetic) or Gaussian mode. Many high power CO_2 lasers and solid state lasers generally produce a complicated mixtures of the two lowest-order spatial modes(Gregson and Sanders, 1974) TEM_{00} and TEM_{01}, the latter often referred to as the doughnut mode. The Gaussian source corresponds to the case $A=1$ and is shown in Fig. 1(b) along with the characteristic radial dimension d. In this case the maximum irradiance occurs at the center of the profile and is generally the reason why the Gaussian source is often preferred for most industrial materials processing applications involving highly reflective surfaces. The doughnut source shown in Fig. 1(a) corresponds to the case $A=0$.

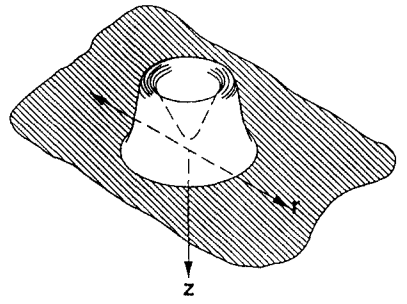

(a) doughnut

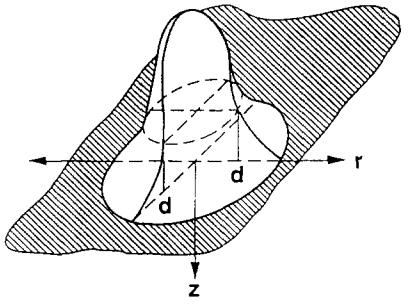

(b) Gaussian

Fig. 1 Spatial profiles of laser sources

This source represents a situation in which the maximum irradiance is not only reduced from that of the Gaussian source but is concentrated in a ring of doughnut shape. The doughnut source is generally useful in situations where the concentrated ring of energy leads to better edge quality in various cutting operations although it is more difficult to focus than Gaussian source.

The governing Eq. (5) for an axisymmetric orthotropic medium with the assumption of constant properties can be rewritten as follows:

$$\frac{\partial^2 T}{\partial r^2}+\frac{1}{r}\frac{\partial T}{\partial r}+\varepsilon\frac{\partial^2 T}{\partial z^2}=\frac{1}{c^2}\frac{\partial^2 T}{\partial t^2}+\frac{1}{\alpha_r}\frac{\partial T}{\partial t} \tag{8}$$

where

$$\varepsilon=\frac{k_z}{k_r},\ \alpha_r=\frac{k_r}{\rho c_p},\ \text{and}\ c^2=\frac{\alpha_r}{\tau}$$

The boundary and initial conditions may be expressed as

$$-k_z\frac{\partial T}{\partial z}=q_o\left[f(t)+\tau\frac{df(t)}{dt}\right]\cdot\left[A+(1-A)\frac{r^2}{d^2}\right]e^{-\frac{r^2}{d^2}} \quad at\ z=0 \tag{9}$$

$$T\rightarrow T_0 \quad as\ r,\ z\rightarrow\infty \tag{10}$$

$$\frac{\partial T}{\partial r}=0 \quad at\ r=0 \tag{11}$$

$$T=T_0 \quad at\ t=0 \tag{12}$$

$$\frac{\partial T}{\partial t}=0 \quad at\ t=0 \tag{13}$$

For convenience in the subsequent analysis, the following dimensionless quantities are introduced.

$$\rho=\frac{cr}{2\alpha_r} \tag{14}$$

the dimensionless radial coordinate;

$$\eta=\frac{cz}{2\alpha_r} \tag{15}$$

the dimensionless axial coordinate;

$$\xi=\frac{c^2 t}{2\alpha_r} \tag{16}$$

the dimensionless time;

$$\mu=\frac{2\alpha_r}{cd} \tag{17}$$

the dimensionless reciprocal of d; and

$$\theta(\rho,\ \eta,\ \xi)=\frac{T(r,\ z,\ t)-T_0}{q_0\alpha_r/k_rc} \tag{18}$$

the dimensionless temperature.

With dimensionless quantities, we obtain the following system of equations

$$\frac{\partial^2\theta}{\partial\rho^2}+\frac{1}{\rho}\frac{\partial\theta}{\partial\rho}+\varepsilon\frac{\partial^2\theta}{\partial\eta^2}=2\frac{\partial\theta}{\partial\xi}+\frac{\partial^2\theta}{\partial\xi^2} \quad in\ \rho>0,\ \eta>0,\ \xi>0 \tag{19}$$

$$\frac{\partial\theta}{\partial\eta}=-\frac{2}{\varepsilon}F(\xi)[A+(1-A)\mu^2\rho^2]e^{-\mu^2\rho^2} \quad at\ \eta=0 \tag{20}$$

$$\theta\rightarrow 0 \quad as\ \rho,\ \eta\rightarrow\infty \tag{21}$$

$$\frac{\partial\theta}{\partial\rho}=0 \quad at\ \rho=0 \tag{22}$$

$$\theta=0 \quad at\ \xi=0 \tag{23}$$

$$\frac{\partial\theta}{\partial\xi}=0 \quad at\ \xi=0 \tag{24}$$

where the function $F(\xi)$ represents the dimensionless temporal profile of the boundary flux. Solutions of this system for prescribed $F(\xi)$ and values of A are presented in the following equations.

3. Analysis

We examine the solution of the hyperbolic system Eqs. (19)~(24) for several different types of applied surface sources, including a continuous Gaussian source, continuous doughnut source, continuous mixed source, single pulse Gaussian source, single pulse doughnut source and single pulse mixed source. The solutions for the corresponding parabolic(i. e. Fourier) system are listed in the Appendix. Here, we follow the procedure employed in the previous work(Kim et al., 1990) which dealt with an isotropic medium.

3.1 Continuous caussian source

In the case of a continuous Gaussian source $f(t)=H(t)$, $A=1$, the dimensionless form of Eq. (9) becomes

$$\frac{\partial\theta}{\partial\eta}=-[2H(\xi)+\delta(\xi)]\frac{e^{-\mu^2\rho^2}}{\varepsilon} \quad at\ \eta=0 \tag{25}$$

In order to solve Eq. (19) subject to Eqs. (21)~(24) and (25) we introduce the following integral transform pair on the ρ-variable

Transform :

$$\bar{\theta}(\beta,\ \eta,\ \xi)=\int_{\rho'=0}^{\infty}\rho' J_0(\beta\rho')\cdot\theta(\rho',\ \eta,\ \xi)d\rho' \tag{26}$$

Inversion :

$$\theta(\rho,\ \eta,\ \xi)=\int_{\beta=0}^{\infty}\beta J_0(\beta\rho)\bar{\theta}(\beta,\ \eta,\ \xi)d\beta \tag{27}$$

where $J_0(\beta\rho)$ is the zeroth order Bessel function of the first kind. In order to transform the system Eqs. (19)~(24) we operate on these equations with

$$\int_{\rho'=0}^{\infty}\rho' J_0(\beta\rho')d\rho' \tag{28}$$

which gives

$$\varepsilon\frac{\partial^2\bar{\theta}}{\partial\eta^2}=2\frac{\partial\bar{\theta}}{\partial\xi}+\frac{\partial^2\bar{\theta}}{\partial\xi^2}+\beta^2\bar{\theta} \quad in\ \eta>0,\ \xi>0 \tag{29}$$

$$\frac{\partial\bar{\theta}}{\partial\eta}=-[2H(\xi)+\delta(\xi)]\frac{g(\beta)}{\varepsilon} \quad at\ \eta=0 \tag{30}$$

$$\bar{\theta}\to 0 \quad as\ \eta\to\infty \tag{31}$$

$$\bar{\theta}=0 \quad at\ \xi=0 \tag{32}$$

$$\frac{\partial\bar{\theta}}{\partial\xi}=0 \quad at\ \xi=0 \tag{33}$$

where the function $g(\beta)$ is defined by

$$g(\beta)=\int_{\rho'=0}^{\infty}\rho' e^{-\mu^2\rho'^2}J_0(\beta\rho')d\rho' \tag{34}$$

Application of the Laplace transform

$$\tilde{\bar{\theta}}(\beta,\ \eta,\ s)=\int_{\xi'=0}^{\infty}e^{-s\xi'}\bar{\theta}(\beta,\ \eta,\ \xi')d\xi' \tag{35}$$

to Eqs. (29)~(33) gives the following system for the double transform

$$\frac{d^2\tilde{\bar{\theta}}}{d\eta^2}-\frac{(\beta^2+s^2+2s)}{\varepsilon}\tilde{\theta}=0 \quad in\ \eta>0 \tag{36}$$

$$\frac{d\tilde{\bar{\theta}}}{d\eta}=-\left[\frac{2}{s}+1\right]\frac{g(\beta)}{\varepsilon} \quad at\ \eta=0 \tag{37}$$

$$\tilde{\bar{\theta}}\to 0 \quad as\ \eta\to\infty \tag{38}$$

The solution to Eq. (36) subject to Eqs. (37) and (38) gives

$$\tilde{\theta}(\beta,\ \eta,\ s)=\left[\frac{2}{s}+1\right]\frac{e^{-\omega\eta}g(\beta)}{\omega\varepsilon} \tag{39}$$

where

$$\omega=\frac{\sqrt{(s+1)^2+\beta^2-1}}{\sqrt{\varepsilon}} \tag{40}$$

Utilizing the inverse Laplace transform

$$L^{-1}\left\{\frac{1}{s}\tilde{h}(s\mp a)\right\}=\int_{\xi'=0}^{\xi}e^{\pm a\xi'}\tilde{h}(\xi')d\xi' \tag{41}$$

the term $\frac{e^{-\omega\eta}}{\omega s}$ appearing in Eq. (39) is inverted as

$$L^{-1}\left\{\frac{e^{-\omega\eta}}{\omega s}\right\}=\begin{cases}\sqrt{\varepsilon}\displaystyle\int_{\xi'=0}^{\xi}e^{-\xi'}I_0\left(\sqrt{1-\beta^2}\sqrt{\xi'^2-\frac{\eta^2}{\varepsilon}}\right)H\left(\xi'-\frac{\eta}{\sqrt{\varepsilon}}\right)d\xi' & for\ 0\le\beta\le 1\\ \sqrt{\varepsilon}\displaystyle\int_{\xi'=0}^{\xi}e^{-\xi'}J_0\left(\sqrt{\beta^2-1}\sqrt{\xi'^2-\frac{\eta^2}{\varepsilon}}\right)H\left(\xi'-\frac{\eta}{\sqrt{\varepsilon}}\right)d\xi' & for\ 1\le\beta\le\infty\end{cases} \tag{42}$$

The integral defined by Eq. (34) is determined as

$$g(\beta)=\frac{e^{-\frac{\beta^2}{4\mu^2}}}{2\mu^2} \tag{43}$$

Finally, the double inversion of Eq. (39) gives the desired solution as

$$\theta(\rho,\ \eta,\ \xi)=\frac{e^{-\xi}}{2\sqrt{\varepsilon}}G_1(\rho,\ \eta,\ \xi)H\left(\xi-\frac{\eta}{\sqrt{\varepsilon}}\right)+\frac{1}{\sqrt{\varepsilon}}\int_{\xi'=\frac{\eta}{\sqrt{\varepsilon}}}^{\xi}e^{-\xi'}\cdot G_1(\rho,\ \eta,\ \xi')d\xi' \tag{44}$$

where

$$G_1(\rho,\ \eta,\ \xi)=\frac{1}{\mu^2}\left\{\int_{\beta=0}^{1}\beta e^{-\frac{\beta^2}{4\mu^2}}J_0(\beta\rho)I_0\left(\sqrt{1-\beta^2}\sqrt{\xi^2-\frac{\eta^2}{\varepsilon}}\right)d\beta+\int_{\beta=1}^{\infty}\beta e^{-\frac{\beta^2}{4\mu^2}}J_0(\beta\rho)J_0\left(\sqrt{\beta^2-1}\sqrt{\xi^2-\frac{\eta^2}{\varepsilon}}\right)d\beta\right\} \tag{45}$$

and $I_o(x)$ is the modified Bessel function of the first kind of order zero. The integrals in Eq. (45) can be evaluated numerically(IMSL, 1989).

3.2 Continuous doughnut source

The doughnut source depicted in Fig. 1(a) has a minimum that corresponds to zero heat flux at the center. In this case $f(t)=H(t)$, $A=0$ and Eq. (20) reduces to

$$\frac{\partial\theta}{\partial\eta}=-\frac{[2H(\xi)+\delta(\xi)]}{\varepsilon}\mu^2\rho^2e^{-\mu^2\rho^2} \tag{46}$$

$$at\ \eta=0$$

Following the solution procedure as outlined for the continuous Gaussian source, with a careful interpretation of the integral

$$\int_{\rho'=0}^{\infty}\rho'^3e^{-\mu^2\rho'^2}J_0(\beta\rho')d\rho'=\frac{1}{2\mu^4}\left[1-\frac{\beta^2}{4\mu^2}\right]e^{-\frac{\beta^2}{4\mu^2}} \tag{47}$$

we find the following dimensionless temperature

$$\theta(\rho,\ \eta,\ \xi)=\frac{e^{-\xi}}{2\sqrt{\varepsilon}}G_2(\rho,\ \eta,\ \xi)H\left(\xi-\frac{\eta}{\sqrt{\varepsilon}}\right)+\frac{1}{\sqrt{\varepsilon}}\int_{\xi'=\frac{\eta}{\sqrt{\varepsilon}}}^{\xi}e^{-\xi'}G_2(\rho,\ \eta,\ \xi')d\xi' \tag{48}$$

where

$$G_2(\rho,\ \eta,\ \xi)=\frac{1}{\mu^2}\left\{\int_{\beta=0}^{1}\beta\left(1-\frac{\beta^2}{4\mu^2}\right)e^{-\frac{\beta^2}{4\mu^2}}J_0(\beta\rho)\times I_0\left(\sqrt{1-\beta^2}\sqrt{\xi^2-\frac{\eta^2}{\varepsilon}}\right)d\beta+\int_{\beta=1}^{1}\beta\left(1-\frac{\beta^2}{4\mu^2}\right)e^{-\frac{\beta^2}{4\mu^2}}J_0(\beta\rho)\quad\times J_0\left(\sqrt{\beta^2-1}\sqrt{\xi^2-\frac{\eta^2}{\varepsilon}}\right)d\beta\right\} \tag{49}$$

3.3 Continuous mixed source

The temperature response to the continuous mixed source may be written as a combination of the solutions given in Eqs. (44) and (48) as

$$\theta(\rho,\ \eta,\ \xi)=\frac{e^{-\xi}}{2\sqrt{\varepsilon}}[AG_1(\rho,\ \eta,\ \xi)+(1-A)G_2(\rho,\ \eta,\ \xi)]H\left(\xi-\frac{\eta}{\sqrt{\varepsilon}}\right)+\frac{1}{\sqrt{\varepsilon}}\int_{\xi'=\frac{\eta}{\sqrt{\varepsilon}}}^{\xi}e^{-\xi'}[AG_1(\rho,\ \eta,\ \xi')+(1-A)G_2(\rho,\ \eta,\ \xi')]d\xi' \tag{50}$$

3.4 Single pulse Gaussian source

The temporal profile for a single pulse source activated for a small time period Δt is

$$f(t)=H(t)-H(t-\Delta t) \tag{51}$$

and Eq. (20) becomes

$$\frac{\partial\theta}{\partial\eta}=-[2\{H(\xi)-H(\xi-\Delta\xi)\}+\delta(\xi)-\delta(\xi-\Delta\xi)]\frac{e^{-\mu^2\rho^2}}{\varepsilon}\quad at\ \eta=0 \tag{52}$$

In this situation the surface $\eta=0$ is irradiated with a Gaussian source which is temporally square having width $\Delta\xi$. Although the real temporal profile of a pulsed laser does not possess such sharp discontinuities in time, the temporally square profile remains a useful approximation for

the most heat transfer analyses. The following temperature response to a pulsed Gaussian source is obtained from the solution procedure as previously outlined.

$$\theta(\rho,\ \eta,\ \xi)=\frac{e^{-\xi}}{2\sqrt{\varepsilon}}\left[G_1(\rho,\ \eta,\ \xi)H\left(\xi-\frac{\eta}{\sqrt{\varepsilon}}\right)-e^{\Delta\xi}G_1(\rho,\ \eta,\ \xi-\Delta\xi)H\left(\xi-\Delta\xi-\frac{\eta}{\sqrt{\varepsilon}}\right)\right]$$
$$+\frac{1}{\sqrt{\varepsilon}}\int_{\xi'=\frac{\eta}{\sqrt{\varepsilon}}}^{\xi}e^{-\xi}G_1(\rho,\ \eta,\ \xi')d\xi'-\frac{1}{\sqrt{\varepsilon}}\int_{\xi'=\frac{\eta}{\sqrt{\varepsilon}}}^{\xi-\Delta\xi}e^{-\xi'}G_1(\rho,\ \eta,\ \xi')d\xi' \tag{53}$$

3.5 Single pulse doughnut source

For the case of a pulsed doughnut source, the temperature profile is found to be

$$\theta(\rho,\ \eta,\ \xi)=\frac{e^{-\xi}}{2\sqrt{\varepsilon}}\left[G_2(\rho,\ \eta,\ \xi)H\left(\xi-\frac{\eta}{\sqrt{\varepsilon}}\right)-e^{\Delta\xi}G_2(\rho,\ \eta,\ \xi-\Delta\xi)H\left(\xi-\Delta\xi-\frac{\eta}{\sqrt{\varepsilon}}\right)\right]$$
$$+\frac{1}{\sqrt{\varepsilon}}\int_{\xi'=\frac{\eta}{\sqrt{\varepsilon}}}^{\xi}e^{-\xi}G_2(\rho,\ \eta,\ \xi')d\xi'-\frac{1}{\sqrt{\varepsilon}}\int_{\xi'=\frac{\eta}{\sqrt{\varepsilon}}}^{\xi-\Delta\xi}e^{-\xi'}G_2(\rho,\ \eta,\ \xi')d\xi' \tag{54}$$

3.6 Single pulse mixed source

The temperature response to a pulsed mixed source is a combination of the temperature profile given in Eq. (53) and (54).

$$\theta(\rho,\ \eta,\ \xi)=\frac{e^{-\xi}}{2\sqrt{\varepsilon}}\left[\{AG_1(\rho,\ \eta,\ \xi)+(1-A)G_2(\rho,\ \eta,\ \xi)\}H\left(\xi-\frac{\eta}{\sqrt{\varepsilon}}\right)\right.$$
$$\left.-\{AG_1(\rho,\ \eta,\ \xi-\Delta\xi)+(1-A)G_2(\rho,\ \eta,\ \xi-\Delta\xi)\}e^{\Delta\xi}H\left(\xi-\Delta\xi-\frac{\eta}{\sqrt{\varepsilon}}\right)\right]$$
$$+\frac{1}{\sqrt{\varepsilon}}\int_{\xi'=\frac{\eta}{\sqrt{\varepsilon}}}^{\xi}e^{-\xi'}[AG_1(\rho,\ \eta,\ \xi')+(1-A)G_2(\rho,\ \eta,\ \xi')]d\xi'$$
$$-\frac{1}{\sqrt{\varepsilon}}\int_{\xi'=\frac{\eta}{\sqrt{\varepsilon}}}^{\xi-\Delta\xi}e^{-\xi'}[AG_1(\rho,\ \eta,\ \xi')+(1-A)G_2(\rho,\ \eta,\ \xi')]d\xi' \tag{55}$$

4. Results and Discussion

Numerical computations are performed to examine the behavior of the temperature response in an orthotropic, semi-infinite medium due to axisymmetric surface source with a Gaussian spatial profile.

Here, we present the temperature variations of $\varepsilon=1$ considered in Kim et al.(1990) in order to examine the effects of the conductivity ratio on the temperature distributions in an orthotropic medium compared to the ones in an isotropic medium. Three different values of the conductivity ratio, $\varepsilon=k_z/k_r$ are chosen as $\varepsilon=0.1$, 1(isotropic case), and 10 for comparison.

Figure 2 shows the surface temperature distribution for the three different values of conductivity ratio of $\varepsilon=0.1$, 1 and 10 at dimensionless time of $\xi=0.1$ due to a continuous Gaussian source. It is shown that the temperature response across the irradiated surface generally follows a Gaussian profile. As shown in the figure, the temperature rise at the center of the source, i. e., $\rho=\eta=0$, is more pronounced for both hyperbolic and parabolic cases as the value of ε decreases. The reason follows from the fact that more heat flows along the radial direction than along the axial direction for the smaller values of ε.

Figures. 3(a), 3(b) and 3(c) represent the variation of the temperature along the axis($\rho=0$) due to a continuous Gaussian surface source at dimensionless times of $\xi=0.1$ and 0.4. The temperature distributions for both hyperbolic and parabolic model are quite different from each other. It is demonstrated that the parabolic model predicts instantaneous energy propagation through the material while the hyperbolic model shows the wave nature of the energy propagation. It shows that the thermal penetration depth for both models is getting deeper for larger ε value. This is due to the fact that the energy propagates more rapidly in the axial direction with increasing value of ε. As shown in the figure, the

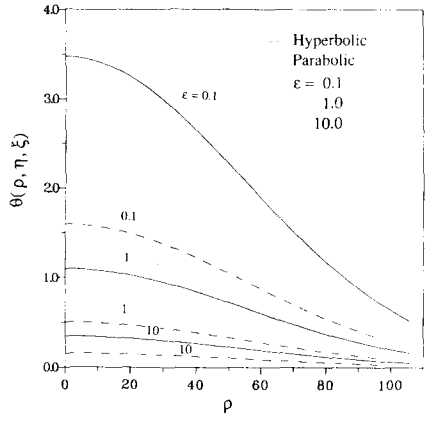

Fig. 2 Temperature distribution for different values of εat the surface, $\eta=0$, plotted as a function of ε the radial position, ρ for a continuous surface heat flux of Gaussian shape at a given time $\xi=0.1$

temperature rise at the center becomes more severe with decreasing value of ε at a given time.

Since hyperbolic model takes into account a thermal inertia effect that accounts for the finite time necessary for the onset of heat flow, a small time must pass prior to the commencement of heat flow. This fact explains why the most significant difference between two models occur close to the surface and the effect is more pronounced at a smaller time.

The temperature variations along the axis due to a temporally square Gaussian pulse at dimensionless time of $\xi=0.7$ and 1.2 are shown in Figs. 4(a), 4(b) and 4(c).

The pulse is activated for a period $\Delta\xi=0.2$. Again, it is shown that the hyperbolic model demonstrates the wave nature since at any one time there are points along the axis which have experienced no temperature change in response to the surface heat flux. A comparison of Figs. 4(a) and 4(b) shows that the localized temperature rise in hyperbolic model is more severe with decreasing value of ε. Figures 4(a) and 4(b) also show that the temperature distributions for both models are quite different from each other. However, Figure 4(c) shows that the two models depict the similar trends up to the axial distance considered in this figure. This is due to the fact that the

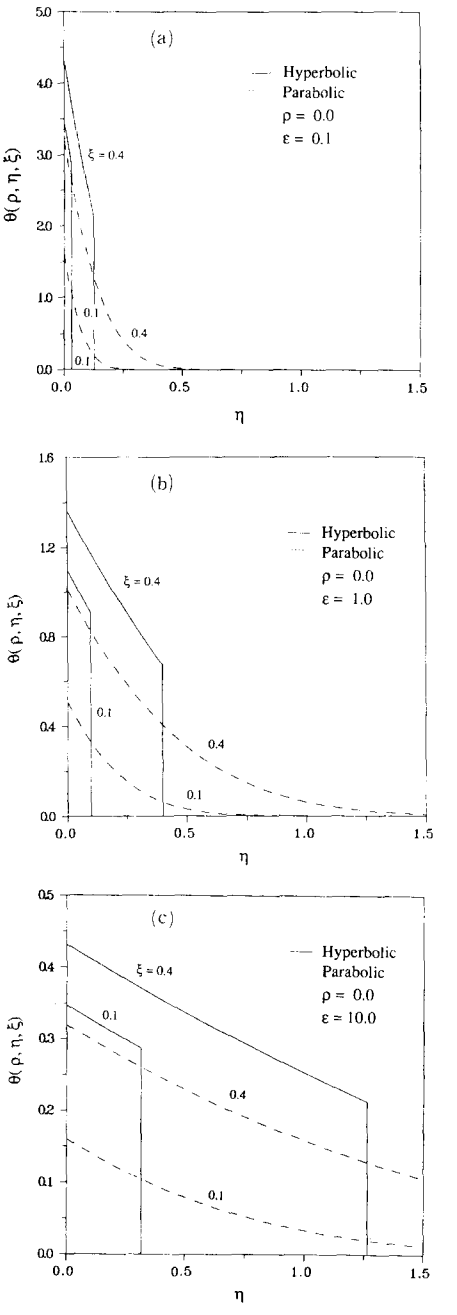

Fig. 3 (a) Variation of center temperature with the axial distance η for a continuous surface heat flux of Gaussian shape and $\varepsilon=0.1$
(b) Variation of center temperature with the axial distance for a continuous surface heat flux of Gaussian shape and $\varepsilon=1.0$
(c) Variation of center temperature with the axial distance η for a continuous surface heat flux of Gaussian shape and $\varepsilon=10.0$

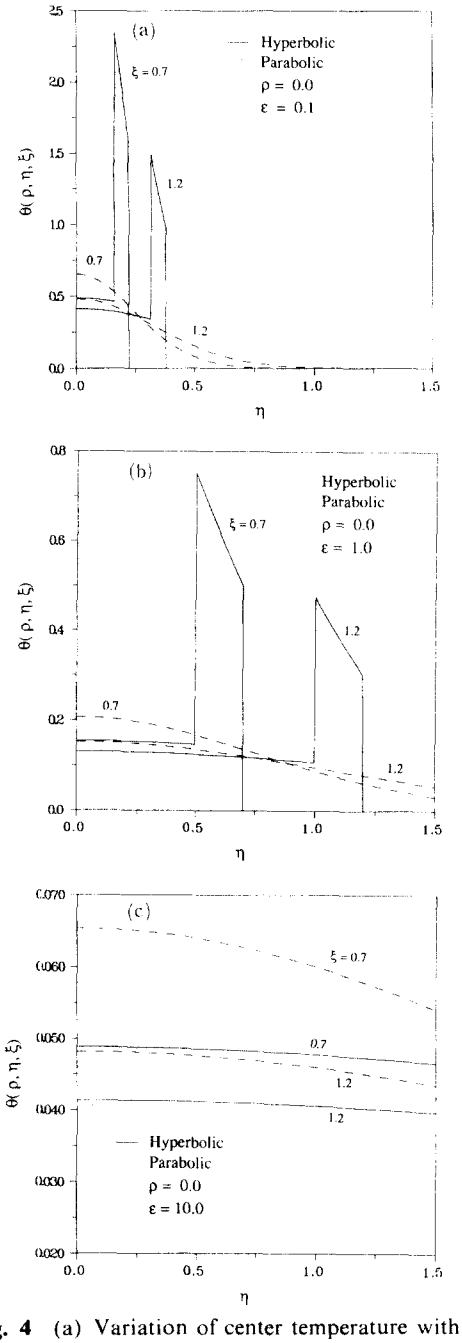

Fig. 4 (a) Variation of center temperature with the axial distance η for a pulsed surface heat flux of Gaussian shape and $\varepsilon=0.1$
(b) Variation of center temperature with the axial distance η for a pulsed surface heat flux of Gaussian shape and $\varepsilon=1.0$
(c) Variation of center temperature with the axial distance η for a pulsed surface heat flux of Gaussian shape and $\varepsilon=10.0$

non-Fourier effect is delayed with increasing value of ε since with a large value of the heat propagation in the axial direction is faster compared to the one with a small value of ε.

For this case($\varepsilon=10$) the wave front in the hyperbolic temperature distribution will show up at a point beyond the axial distance considered in this figure.

Figures 5(a), 5(b) and 5(c) show the variation of temperature with dimensionless time at selected points along the η axis due to a continuous Gaussian source. A comparison of hyperbolic temperature profiles with their parabolic counterparts reveals that the parabolic model predicts instantaneous energy propagation while the hyperbolic model shows discontinuous jumps in temperature followed by a temperature rise which is similar to that predicted by the parabolic model. In Fig. 5(a) it is shown that the wave front in hyperbolic model has not yet arrived at a point $\eta=0.4$ during the time interval chosen in this figure since the wave propagates with a finite speed and the heat propagation speed in axial direction is decreasing with a small value of ε. The hyperbolic temperature distributions show that the arrival time of the wave front at a given axial location, for instance, $\eta=0.4$, is getting shorter as the value of ε is increasing.

Finally, Figures. 6(a), 6(b) and 6(c) show the profiles of the center temperature with dimensionless time at selected points along the axis due to a temporally square Gaussian pulse, which was activated for a period $\Delta\xi=0.2$. Again, the hyperbolic model predicts a thermal wave with a finite speed whereas the parabolic model shows no wave nature. The hyperbolic temperature profile displays a localized severe temperature rise for the period $\Delta\xi=0.2$ and then the temperature drops rapidly. Also, in Fig. 6(a) the thermal wave front has not yet arrived at a point $\eta=0.4$. This fact can be explained by referring to the arguments previously discussed in Fig. 5(a). A comparison of the height of the wave front at $\eta=0$ with the one at $\eta=0.4$ shows that the height of the thermal wave front is diminished along the axis since the thermal wave dissipates its energy by traveling through the medium. The effects of the value of ε

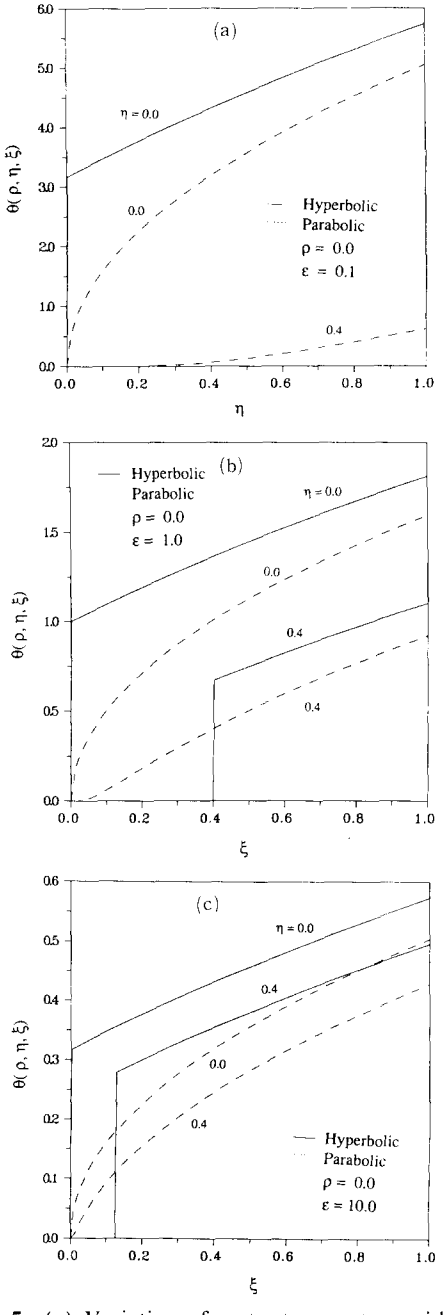

Fig. 5 (a) Variation of center temperature with the time ζ for a continuous surface heat flux of Gaussian shape and $\varepsilon=0.1$
(b) Variation of center temperature with the time ζ for a continuous surface heat flux of Gaussian shape and $\varepsilon=1.0$
(c) Variation of center temperature with the time ζ for a continuous surface heat flux of Gaussian shape and $\varepsilon=10.0$

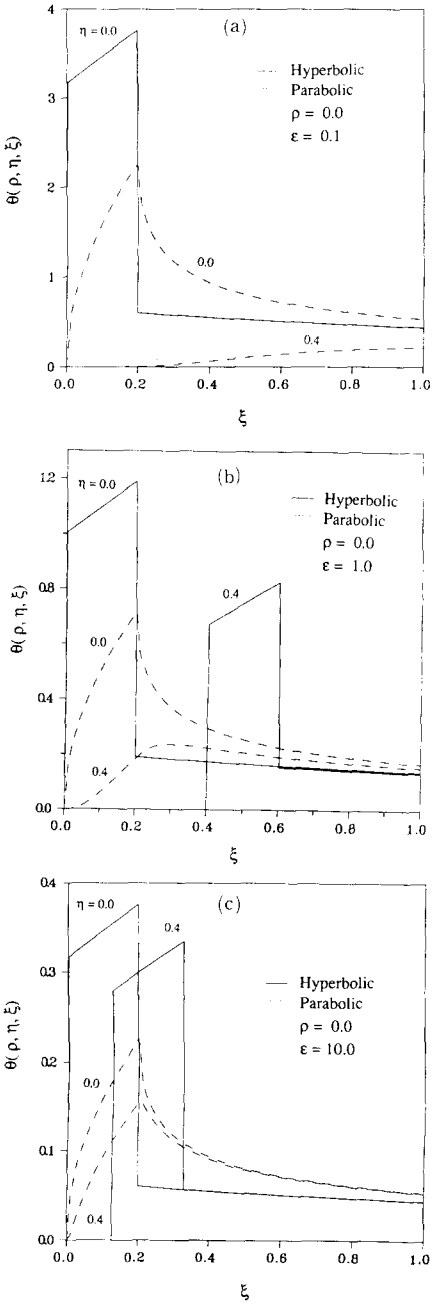

Fig. 6 (a) Variation of center temperature with the time ζ for a pulsed surface heat flux of Gaussian shape and $\varepsilon=0.1$
(b) Variation of center temperature with the time ζ for a pulsed surface heat flux of Gaussian shape and $\varepsilon=1.0$
(c) Variation of center temperature with the time ζ for a pulsed surface heat flux of Gaussian shape and $\varepsilon=10.0$

on the temperature profiles for both models are similar to those in Figs. 5(a), 5(b) and 5(c). The parabolic temperature distributions at $\eta=0$ generally display a smooth increase for the pulse activation period and then a relatively rapid decrease.

5. Conclusion

The transient temperature distribution in an orthotropic, semi-infinite medium due to axisymmetric heat source at the boundary surface has been determined with a hyperbolic heat conduction model. Several different types of applied surface sources are considered. The results show that the localized temperature rise in the case of a pulsed source becomes more drastic with decreasing value of ε compared with the care of an isotropic medium of $\varepsilon=1$. It is shown that the temperature distribution in an orthotropic medium depends on the value of the conductivity ratio and the profile behaves unlike the case in an isotropic medium. The predictions based on an isotropic medium may lead to an erroneous result when the medium behaves like an orthotropic medium.

Acknowledgement

One of the authors(W. S. Kim) wishes to acknowledge the support received from the Korean Science Foundation through Grant No. 923-0900-001-2.

References

Baumeister, K. J. and Hamill, T. D., 1969, "Hyperbolic Heat-Conduction Equation-A Solution for the Semi-Infinite Body Problem," *ASME J. Heat Transfer,* Vol. 91, pp. 543~548.

Frankel, J. I., Vick, B. and Ozisik, M. N., 1987, "General Formulation and Analysis of Hyperbolic Heat Coduction in Composite Media," *Int. J. Heat Mass Transfer,* Vol. 30, pp. 1293~1305.

Gembarovic, J. and Majernik, V., 1987, "Determination of Thermal Parameters of Relaxation Materials," *Int. J. Heat Mass Transfer,* Vol. 30, pp. 199~201.

Glass, D. E., Ozisik, M. N. and Kim, W. S., 1990, "Hyperbolic Stefan Problem with Applied Surface Heat Flux and Temperature-Dependent Thermal Conductivity," *Num. Heat Transfer,* Vol. 18, pp. 503~516.

Glass, D. E., Ozisik, M. N., McRae, D. S. and Vick, B., 1986, "Hyperbolic Heat Conduction with Temperature-Dependent Thermal Conductivity," *J. Appl. Phys.,* Vol. 59, pp. 1861~1865.

Glass, D. E., Ozisik, M. N. and Vick, B., 1985, "Hyperbolic Heat Conduction with Surface Radiation," *Int. J. Heat Mass Transfer,* Vol. 28, pp. 1823~1830.

Gregson, V. G. and Sanders, B. A., 1974, "A Physical Model of Laser Heat Treatment," *Proc. 1974 Electro-Optic Systems Design Conf., Industrial and Scientific Management,* pp. 237~243.

IMSL MATH/LIBRARY Version 2.1, 1989, Houston, Texas.

Kaminski, W., 1990, "Hyperbolic Heat Conduction Equation for Materials with a Nonhomogeneous Inner Structure," *ASME J. Heat Transfer*, Vol. 112, pp. 555~560.

Kim, W. S., Hector, Jr. L. G. and Ozisik, M. N., 1990, "Hyperbolic Heat Conduction Due to Axisymmetric Continuous or Pulsed Surface Heat Sources," *J. Appl. phys.* Vol. 68, pp. 5478~5485.

Maxwell, J. C., 1867, "On the Dynamical Theory of Gases," *Philos. Trans. R. Soc.* London, Vol. 157, pp 49~88.

Ozisik, M. N., 1993, *Heat Conduction,* 2nd ed., John-Wiley & Sons, New York.

Peshkov, V., 1944, "Second Sound in He II," *Journal of Physics,* USSR, Vol. 8, p. 381.

Tzou, D. Y., 1989, "On the Thermal Shock Wave Induced by a Moving Heat Source," *ASME J. Heat Transfer,* Vol. III, pp. 232~238.

Tzou, D. Y., 1990, "Thermal Shock Waves Induced by a Moving Crack-a Heat Flux Formulation," *Int. J. Heat Mass Transfer,* Vol. 33, pp. 877~885.

Appendix

Fourier Heat Conduction Solutions

They are listed here for the convenience of

comparison with their non-Fourier counterparts discussed in the body of the paper.

Continuous Mixed Source

$$\theta(\rho,\ \eta,\ \xi)=\sqrt{\frac{2}{\pi\varepsilon}}\int_{\xi'=0}^{\xi}\{AG_3(\rho,\ \eta,\ \xi')+(1-A)G_4(\rho,\ \eta,\ \xi')\}\frac{d\xi'}{\sqrt{\xi'(1+2\mu^2\xi')}} \tag{A1}$$

where

$$G_3(\rho,\ \eta,\ \xi)=\exp\left[-\left(\frac{\eta^2}{2\varepsilon\xi}+\frac{\mu^2\rho^2}{1+2\mu^2\xi}\right)\right] \tag{A2}$$

$$G_4(\rho,\ \eta,\ \xi)=\left[1-\frac{1}{1+2\mu^2\xi}\left(1-\frac{\mu^2\rho^2}{1+2\mu^2\xi}\right)\right]G_3(\rho,\ \eta,\ \xi) \tag{A3}$$

Continuous Gaussian Source-Set $A=1$ in Eq. (A1)

Continuous Doughnut Source-Set $A=0$ in Eq. (A1)

Single Pulse Mixed Source

$$\theta(\rho,\ \eta,\ \xi)=\sqrt{\frac{2}{\pi\varepsilon}}\left\{\int_{\xi'=0}^{\xi}[AG_3(\rho,\ \eta,\ \xi')+(1-A)G_4(\rho,\ \eta,\ \xi')]\times\frac{d\xi'}{\sqrt{\xi'(1+2\mu^2\xi')}}\right.$$
$$\left.-\int_{\xi'=0}^{\xi-\Delta\xi}[AG_3(\rho,\ \eta,\ \xi')+(1-A)G_4(\rho,\ \eta,\ \xi')]\times\frac{d\xi'}{\sqrt{\xi'(1+2\mu^2\xi')}}\right. \tag{A4}$$

Single Pulse Gaussian Source-Set $A=1$ in Eq. (A4)

Single Pulse Doughnut Source-Set $A=0$ in Eq. (A4)